International Journal of Nanomedicine

Dovepress
open access to scientific and medical research

Open Access Full Text Article

ORIGINAL RESEARCH

Microarc-oxidized titanium surfaces functionalized with microRNA-21-loaded chitosan/hyaluronic acid nanoparticles promote the osteogenic differentiation of human bone marrow mesenchymal stem cells

This article was published in the following Dove Press journal:
International Journal of Nanomedicine
27 October 2015
Number of times this article has been viewed

Zhongshan Wang[1,*]
Guangsheng Wu[2,3,*]
Zhihong Feng[1]
Shizhu Bai[1]
Yan Dong[1]
Guofeng Wu[1]
Yimin Zhao[1]

[1]State Key Laboratory of Military Stomatology, Department of Prosthetic Dentistry, [2]State Key Laboratory of Military Stomatology, Department of Periodontology, School of Stomatology, The Fourth Military Medical University, Xi'an, People's Republic of China; [3]Qingdao First Sanatorium, Jinan Military Region, Qingdao, Shandong Province, People's Republic of China

*These authors contributed equally to this work

Abstract: Dental implants have been widely used for the replacement of missing teeth in the clinic, but further improvements are needed to meet the clinical demands for faster and tighter osseointegration. In this study, we fabricated safe and biocompatible chitosan (CS)/hyaluronic acid (HA) nanoparticles to deliver microRNA-21 (miR-21) and thereby accelerate osteogenesis in human bone marrow mesenchymal stem cells (hBMMSCs). The CS/HA/miR-21 nanoparticles were cross-linked with 0.2% gel solution onto microarc oxidation (MAO)-treated titanium (Ti) surfaces to fabricate the miR-21-functionalized MAO Ti surface, resulting in the development of a novel coating for reverse transfection. To characterize the CS/HA/miR-21 nanoparticles, their particle size, zeta potential, surface morphology, and gel retardation ability were sequentially investigated. Their biological effects, such as cell viability, cytotoxicity, and expression of osteogenic genes by hBMMSCs on the miR-21-functionalized MAO Ti surfaces, were evaluated. Finally, we explored appropriate CS/HA/miR-21 nanoparticles with a CS/HA ratio of 4:1 and N/P ratio 20:1 for transfection, which presented good spherical morphology, an average diameter of 160.4±10.75 nm, and a positive zeta potential. The miR-21-functionalized MAO Ti surfaces demonstrated cell viability, cytotoxicity, and cell spreading comparable to those exhibited by naked MAO Ti surfaces and led to significantly higher expression of osteogenic genes. This novel miR-21-functionalized Ti implant may be used in the clinic to allow more effective and robust osseointegration.

Keywords: titanium implants, microarc oxidation, human bone marrow MSCs, microRNA, nanoparticles, osteogenic differentiation

Introduction

Dental implants have been widely used for the replacement of missing teeth.[1] It is widely believed that the surface topography of biomedical implants plays a critical role in osseointegration and clinical success. Micro- and nanoscale topographies have been proven to facilitate interactions with bone cells.[2,3] In particular, the microarc oxidation (MAO) titanium (Ti) surface has been widely used in the dental clinic and has been shown to have favorable effects on implant osseointegration through the induction of apatite deposition and promotion of osteoblast functions.[4,5] However, some conditions, such as diabetes, osteoporosis, and radioactive therapy after oral tumor resection, can affect the bioactivity of bone cells and bone tissues, eventually resulting in osteopenia and impaired healing of fractures.[6,7] Therefore, further improvements are needed to meet the clinical demands for faster and tighter osseointegration.

Correspondence: Yimin Zhao
State Key Laboratory of Military Stomatology, Department of Prosthetic Dentistry, School of Stomatology, The Fourth Military Medical University, 145 West Changle Road, Xi'an 710032, People's Republic of China
Tel +86 29 8477 6465
Fax +86 29 8477 6465
Email zhaoymdentist@163.com

An effective strategy for promoting osseointegration involves the loading of advantageous biomolecules, such as growth factors and bioactive substances, onto an implant surface to stimulate cellular differentiation, migration, and gene expression, further promoting extracellular matrix deposition and exerting osteoinductive effects.[8–10] It is also necessary to enhance the reservoir capacity of the Ti implant surface to load more advantageous biomolecules. Interestingly, the Ti topographies formed by MAO treatment that are widely used in the clinic demonstrate evenly distributed micropores, which facilitate an enlarged surface area for drug attachment and retention.[3] For example, the MAO Ti surface has been prepared for the loading of poly(L-lactic acid) nanoparticles containing antibacterial compounds cross-linked with a gelatin solution and attached onto the micropores of the MAO Ti surface.[11] Wikesjö et al[9] loaded bone morphogenetic protein 2 onto the MAO Ti surface by physical adsorption and successfully observed increased local bone formation.[9] Thus, we can expect that the loading of more effective biomolecules with gene regulatory functions onto the MAO Ti surface will result in superior biological performance.

Over the last decade, microRNA (miRNA) molecules, with a length of only 20–30 nucleotides, have emerged as critical regulators of endogenous genes in both somatic and germline lineages through binding primarily to the 3′ untranslated region of their target mRNAs and thereby controlling the mRNA level at the posttranscriptional level.[12,13] As a result, miRNAs function in the natural differentiation pathway and provide a potentially less harmful strategy to control the differentiation of stem cells in vivo.[14,15] Several reports have described the regulatory effect of miRNAs on osteogenesis. One of the most studied miRNAs, miRNA-21 (miR-21), is recognized as a versatile miRNA involved in many biological processes.[16] miR-21 has been found to be highly expressed during osteogenic differentiation, which indicates that this miRNA may repress stemness maintenance in osteoblasts.[16,17] Ourania et al[18] and Meng et al[17] revealed that the overexpression of miR-21 can accelerate osteogenesis and impair adipogenesis in both human umbilical cord mesenchymal stem cells (MSCs) and human bone marrow MSCs (hBMMSCs); miR-21 may exert its osteogenic function through the PI3K-AKT-GSK3β pathway via the stabilization and accumulation of β-catenin.[17]

A key issue in the therapeutic application of miRNAs is safe and highly efficient transfection. Vectors are normally required for the stabilization and efficient delivery of miRNAs.[19] Nonviral gene-delivery systems, such as chitosan (CS)/hyaluronic acid (HA) nanoparticles,[20–23] have been proposed as safer alternatives to viral vectors due to their good biocompatibility, biodegradability, high stability, and minimal host immune response.[20] The positive charges of CS contribute to electrostatic interactions with negatively charged substances, which are also responsible for the capacity of CS to interact with the negatively charged cell surfaces.[24] HA is a natural, anionic polysaccharide that is naturally found in humans, and the natural biomineralization process of HA exerts vital functions in bone and tooth development.[25,26] As a viscous gel, HA has been widely used for cell scaffolding and drug delivery.[22,27] A single application of CS presents a lack of stability due to its low water solubility at physiological pH,[28,29] and the inclusion of an anionic polymer (HA) appears to increase the stability of the particles in plasma and induce an even size distribution of nanoparticles.[23,28–30] In addition, HA has the ability to bind various cellular receptors, such as CD44, which is expressed in normal mammalian cells and cancerous cells.[30] This ability would increase the transfection efficiency of target cells and reduce side effects.[29] In this study, HA was associated with CS through polyelectrolyte complexion and formed CS/HA nanoparticles for the loading and delivery of miR-21. The MAO Ti surfaces were then coated with CS/HA/miR-21 nanoparticles using a 0.2% gel solution,[11] and the miR-21-functionalized MAO Ti surfaces were then fabricated.

In this work, we took advantage of the function of miR-21 as an efficient gene regulator and then fabricated CS/HA nanoparticles as a safe means of developing vectors to deliver transfection agents. We then successfully loaded CS/HA/miR-21 nanoparticles onto the MAO Ti surface by cross-linking using a 0.2% gel solution. Furthermore, we successfully isolated and identified hBMMSCs and evaluated the transgene expression efficacy and cytotoxicity of hBMMSCs on miR-21-functionalized MAO Ti surfaces in vitro. We are confident that this novel coating on the MAO surfaces of Ti implants will provide a new approach for achieving rapid and tighter osseointegration in clinical settings.

Materials and methods

Materials

CS with a molecular weight of 100 kDa and a deacetylation degree of 90% was purchased from JINKE Company Limited (Zhejiang, People's Republic of China). HA, with a molecular weight of 10 kDa, was obtained from Shandong C. P. Freda Pharmaceutical Co., Ltd. (Shandong, People's Republic of China). The miR-21 and negative control oligonucleotides were purchased from Shanghai GenePharma Co, Ltd. (Shanghai, People's Republic of China). Gelatin powder

(type A) was purchased from Sigma-Aldrich (St Louis, MO, USA). Pure Ti (1.5 mm in thickness and 20 mm in diameter) was purchased from the Northwest Institute for Nonferrous Metal Research (Xi'an, People's Republic of China). Alpha Minimum Essential Medium (α-MEM) and fetal bovine serum were obtained from HyClone (Thermo Fisher Scientific, Waltham, MA, USA). Fluorescently labeled monoclonal antibodies, including STRO-1, CD146, CD34, and CD45, were purchased from BioLegend (San Diego, CA, USA).

Preparation of CS/HA/miR-21 nanoparticles

CS/HA nanoparticles were produced as described previously.[20,23] In brief, CS was dissolved in 2% acetic acid at a concentration of 1% (w/v) (pH 5.5), and HA was dissolved in water at 0.1% (w/v) (pH 5.5). Both the CS and HA solutions were filtered through a 0.22 μm membrane and mixed at a rate of 3,000 rpm for 2 hours. Seven different mixtures were prepared with the following CS:HA weight ratios: 1:1, 2:1, 3:1, 4:1, 5:1, 6:1, and 7:1. A constant HA concentration of 11.25 μg/mL was used in all of the mixtures, and the CS concentration was varied as follows: 5.625, 11.25, 22.5, 33.75, 45, 56.25, 67.5, and 78.25 μg/mL. CS/HA/miR-21 nanoparticles were prepared by adding the required volume of 20 μM miR-21 to the CS/HA nanoparticle system by gentle pipetting to form complexes of a selected N/P ratio. The N/P ratio was defined as the molar ratio of the positive CS amino group to the negative RNA phosphate group. The mixture was vortexed rapidly for 3–5 seconds and maintained for 1 hour at room temperature to allow the complete formation of the complexes.

Characterization of CS/HA/miR-21 nanoparticles

Particle size, zeta potential, surface morphology, and gel retardation analyses

The CS/HA nanoparticles were prepared at CS:HA weight ratios of 1:1, 2:1, 3:1, 4:1, 5:1, 6:1, and 7:1, as described in the "Preparation of CS/HA/miR-21 nanoparticles" section. The Z-average hydrodynamic diameter and surface charge of the CS/HA nanoparticles were determined by dynamic light scattering using a Zetasizer Nano ZS instrument (Malvern Instruments Ltd., Malvern, UK) at 25°C. The samples were dried at room temperature after being stained on copper grids and then photographed using a transmission electron microscope (TEM, Hitachi H-600, Hitachi, Tokyo, Japan) to observe the particle morphology. The CS/HA/miR-21 nanoparticles were evaluated by agarose gel electrophoresis. The naked miR-21 and CS/HA/miR-21 nanoparticles with various N/P ratios (1:1, 5:1, 10:1, 15:1, and 20:1) were loaded onto a 2% agarose gel containing ethidium bromide in Tris-borate ethylenediaminetetraacetic acid buffer at pH 8.0. The samples were run on the gel at 120 V for 20 minutes. The gel was then photographed using a GDS-8000 image-acquisition system (UVP, Upland, CA, USA).

Preparation of microarc-oxidized Ti specimens

Commercially pure Ti (1.5 mm in thickness and 20 mm in diameter; Northwest Institute for Nonferrous Metal Research) was polished using waterproof SiC sandpaper from 400 to 1,500 grit, sequentially ultrasonically cleaned in acetone, ethanol, and distilled water, and then air-dried. The polished Ti was treated through an MAO process in an aqueous electrolytic solution containing 0.04 M β-glycerophosphate sodium and 0.2 M calcium acetate using a pulsed direct-current power supply at 400 V DC for 5 minutes with an applied frequency of 600 Hz and a duty cycle of 8%. After ultrasonic cleaning, the samples were air dried and sterilized by cobalt 60 irradiation. The coating was achieved by cross-linking the CS/HA/miR-21 nanoparticles with gelatin on microarc-oxidized Ti. In brief, an appropriate amount of the solution of CS/HA nanoparticles (CS/HA =4:1) was mixed with 20 nm/mL miR-21 solution to produce a solution of CS/HA/miR-21 nanoparticles (N/P =20:1), and the CS/HA/miR-21 nanoparticle solution was then dispersed evenly in an equal quantity of 0.2% gelatin solution (w/v) using 200 μL tips. For the fabrication of miR-21-functionalized MAO Ti specimens at gradient concentrations, 100, 200, and 300 μL suspensions (containing 150, 300, and 450 pmol of miR-21, respectively) were dropped onto each MAO Ti specimen, and the specimens were then oscillated for 10 minutes through an oscillator (HY-2, Hangzhou Huier Experiment Instrument Co., Ltd., Jiangsu, People's Republic of China) to enable penetration of the nanoparticles through the pores of the MAO Ti specimens. The prepared specimens were subsequently dried and stored at 4°C.

Characterization of CS/HA/miR-21 nanoparticle-coated MAO Ti surfaces

The prepared CS/HA/miR-21 nanoparticle-coated MAO Ti specimens and the naked MAO Ti specimens were fixed in 2.5% glutaraldehyde, dehydrated through a graded ethanol series, and freeze-dried. After sputter-coating with gold, the cell morphology was observed with a field emission scanning electron microscope (FE-SEM) instrument (Hitachi S-4800; EIKO Engineering, Tokyo, Japan).

To determine whether miR-21 was stably retained within the CS/HA nanoparticles after the CS/HA/miR-21 nanoparticles were coated onto the MAO Ti specimens, Cy3-labeled miR-21 and fluorescein isothiocyanate (FITC)-labeled CS were used to prepare fluorescence-labeled CS/HA/miR-21 nanoparticles; we prepared CS/HA/miR-21 nanoparticle-coated MAO Ti specimens as described, and the Cy3 and FITC fluorescence signals were then observed under a fluorescence microscope (Olympus, Tokyo, Japan) to evaluate the locations and distribution of miR-21 and the CS/HA nanoparticles, respectively.

Cell culture and characterization of stemness

Primary hBMMSCs were obtained from a 22-year-old female volunteer who was planning to undergo implant placement in the maxilla to replace a first molar.[31] We obtained written informed consent from the volunteer and approval from the Institutional Review Board at Stomatological Hospital of Fourth Military Medical University. Briefly, on the day of implant placement, the drilled hole was carefully curetted, and the harvested cells were cultured in α-MEM supplemented with 10% fetal bovine serum and 1% penicillin/streptomycin (both from Sigma-Aldrich) at 37°C in a humidified atmosphere with 5% CO_2; the culture media were refreshed every 2 days. hBMMSCs at passages 2–5 were used in the subsequent experiment.

A previous method[32] was adopted to assess the presence of cell surface markers of hBMMSCs (P3) through flow cytometry analysis. Briefly, 2×10^5 cells were collected in trypsin and transferred to each microtube, and STRO-1, CD146, CD34, and CD45 antibodies were then added to each microtube according to the manufacturer's instructions; cell suspensions without any added antibody served as controls. All of the microtubes were incubated at 37°C in the dark for 40 minutes and then washed three times with phosphate-buffered saline (PBS). Finally, the cells were resuspended in 300 μL of PBS for the analysis of cell surface markers using a flow cytometry-based cell sorter (Vantage Cell Sorter, Becton & Dickinson, Mountain View, CA, USA). The data were analyzed using the Mod-Fit 2.0 cell cycle analysis program (Becton & Dickinson).

To assess the ability of the cells to undergo osteogenic/adipogenic differentiation, the cells (P3) were seeded into six-well dishes at a concentration of 1×10^5 cells/well and cultured in complete medium until a confluence of 80% was reached. To assess their osteogenic ability, the osteoinductive medium (complete medium supplemented with 50 μg/mL ascorbic acid, 10 nM dexamethasone, and 10 mM β-glycerophosphate) was switched and refreshed every 3 days. To assess the adipogenic ability of the cells, the adipogenic medium (complete medium supplemented with 100 nM dexamethasone, 0.5 mM 3-isobutyl-1-methylxanthine, and 50 mM indomethacin) was also changed and refreshed at 3-day intervals. After a 4-week period of osteogenic induction or a 2-week period of adipogenic induction, the cells were fixed with 4% paraformaldehyde and stained with alizarin red or fresh Oil Red O solution for 15 minutes, respectively. The mineralization nodules and lipid droplets were observed photographically (IX70, Olympus).

Cell transfection and assay of transfection efficiency

To assess the transfection efficiency of CS/HA/miR-21 nanoparticles on MAO Ti surfaces, Cy3-labeled miRNAs and FITC-labeled CS were used to prepare fluorescence-labeled CS/HA/miR-21 nanoparticles. The cells (P3) were seeded onto experimental substrates placed in 12-well plates at a density of 1×10^5 cells/well. Twenty-four hours later, the cells were immediately fixed with 4% paraformaldehyde for 30 minutes at room temperature and washed twice with PBS. The cell nuclei were stained with 4′,6-diamidino-2-phenylindole (DAPI; Sigma-Aldrich), and the FITC, Cy3, and DAPI fluorescence signals were observed through fluorescence microscopy (Olympus) to evaluate the internalization of the CS/HA/miR-21 nanoparticles 24 hours after transfection.

To evaluate the transfection efficiency, fluorescently labeled CS/HA/miR-21 nanoparticles were used, and the cells were transfected as described. At the prescribed time points, the cells were collected in trypsin, washed twice with PBS, and fixed in 1% paraformaldehyde in PBS. The Cy3 fluorescence emitted by the cells after internalization was measured with a flow cytometer (FACScalibur, BD Biosciences, San Jose, CA, USA). As the negative control, untreated MSCs were subjected to the same process. Three biological replicates of each sample were analyzed.

Cell viability

The cell viability was assayed quantitatively by cell counting kit-8 (CCK-8) (Beyotime Institute of Biotechnology, Jiangsu, People's Republic of China). Briefly, hBMMSCs (P3) were seeded onto different experimental substrates placed in 12-well plates at a density of 1×10^5 cells/well. At 24 hours, the medium was changed with 1 mL of regular medium, and the cells were cultured for 24 hours. At the scheduled time, the medium was removed, and the cultures were washed twice with PBS. Then, 720 μL of serum-free α-MEM medium was mixed with 80 μL of CCK-8 reagent, and after the mixture was added to each well, the plate was incubated at 37°C for 3 hours. Subsequently, an aliquot

(150 μL) of supernatant was pipetted into a 96-well plate, and the absorbance at 450 nm was determined using a spectrophotometer (BioTek Instruments Inc., Winooski, VT, USA). A naked MAO surface and a tissue culture plate served as controls, and the assays were repeated three times for each sample (n=3).

Lactate dehydrogenase activity assay

The lactate dehydrogenase (LDH) activity was used as an index of cytotoxicity in the culture medium. Briefly, 24 hours after transfection, the culture medium was collected and centrifuged, and the supernatant was used for the LDH activity assay. The LDH activity was determined spectrophotometrically according to the manufacturer's instructions. Three parallel experiments were conducted for each group.

Cell morphology

The cells (P3) were seeded onto different experimental substrates placed in 12-well plates at a density of 1×10^5 cells/well. After 24 hours of incubation posttransfection, the naked and functionalized MAO Ti specimens with cells cultured on them were washed twice with PBS, fixed in 2.5% glutaraldehyde at 4°C for 2 hours, dehydrated through a graded ethanol series, and freeze-dried. The cell morphology was observed using a FE-SEM instrument (Hitachi S-4800; EIKO Engineering).

Osteogenic gene expression

To investigate the effects of miR-21-functionalized MAO Ti samples on the osteogenesis of the hBMMSCs (P3), we evaluated the expression of osteogenesis-related genes by real-time PCR. Briefly, the cells were seeded onto different experimental substrates placed in 12-well plates at a density of 1×10^5 cells/well. After 24 hours of incubation in regular medium posttransfection, the medium was replaced by osteogenic medium containing 10 mM β-glycerophosphate (Sigma-Aldrich), 50 μg/mL ascorbic acid (Sigma-Aldrich), and 10^{-7} M dexamethasone (Sigma-Aldrich). After culturing for 3, 6, and 9 days, the total RNA was isolated using the TRIzol reagent (Thermo Fisher Scientific), and 1 μg of RNA from each sample was then reverse-transcribed into complementary DNA (cDNA) using the PrimeScript RT reagent kit (Takara, Bio, Otsu, Japan). The expression levels of osteogenesis-related genes, including fibronectin, collagen type Iα1 (*COLI*), collagen type IIIα1 (*COLIII*), runt-related transcription factor 2 (*RUNX2*), osteopontin (*OPN*), and osteocalcin (*OCN*), were quantified using a CFX Connect™ Real-Time PCR Detection System (Bio-Rad Laboratories Inc., CA, USA) with the SYBR Green Master Mix (Roche, Basel, Switzerland). The relative expression levels of the target genes were normalized to the expression of the housekeeping gene. The forward/reverse primers for the selected genes are listed in Table 1.

Table 1 Target cDNA primer sequences used for real-time PCR

COLI
Forward: 5′-GAGGGCCAAGACGAAGACATC-3′
Reverse: 5′-CAGATCACGTCATCGCACAAC-3′
COLIII
Forward: 5′-GGAGCTGGCTACTTCTCGC-3′
Reverse: 5′-GGGAACATCCTCCTTCAACAG-3′
RUNX2
Forward: 5′-TGGTTACTGTCATGGCGGGTA-3′
Reverse: 5′-TCTCAGATCGTTGAACCTTGCTA-3′
OCN
Forward: 5′-CCCAGGCGCTACCTGTATCAA-3′
Reverse: 5′- GGTCAGCCAACTCGTCACAGTC-3′
OPN
Forward: 5′-CAGTTGTCCCCACAGTAGACAC-3′
Reverse: 5′-GTGATGTCCTCGTCTGTAGCATC-3′
GAPDH (housekeeping gene)
Forward: 5′-CTTTGGTATCGTGGAAGGACTC-3′
Reverse: 5′-GTAGAGGCAGGGATGATGTTCT-3′

Abbreviations: cDNA, complementary DNA; *COLI*, collagen type Iα1; *COLIII*, collagen type IIIα1; *RUNX2*, runt-related transcription factor 2; *OPN*, osteopontin; *OCN*, osteocalcin.

Statistical analysis

The results were collected and analyzed with SPSS 17.0 software (IBM Corporation, Armonk, NY, USA), and all of the values are expressed as the means ± standard deviation. The significance level was determined using two-way analysis of variance and Student–Newman–Keuls *q*-tests. A *P*-value of <0.05 was considered statistically significant.

Results

Nanoparticle characterization

Particle size, zeta potential, TEM observation, and gel retardation analyses

The relationship between the weight ratio of CS to HA and the size of the nanoparticles is shown in Figure 1A. A significant decrease in nanoparticle size was found with increasing amounts of CS, and the smallest particle size (160.4±10.75 nm) was obtained with a CS:HA ratio of 4:1. The average zeta potential of the CS/HA nanoparticles became more positive with an increase in the amount of CS within the polyelectrolyte complex. The highest zeta potential was obtained for CS:HA weight ratios of 7:1, yielding zeta values of approximately 34.9±3.56 mV. The morphologies of the CS/HA nanoparticles were observed by TEM (Figure 1B), and the typical images indicated that most of the CS/HA nanoparticles were spherical in shape and finely dispersed in the field of vision.

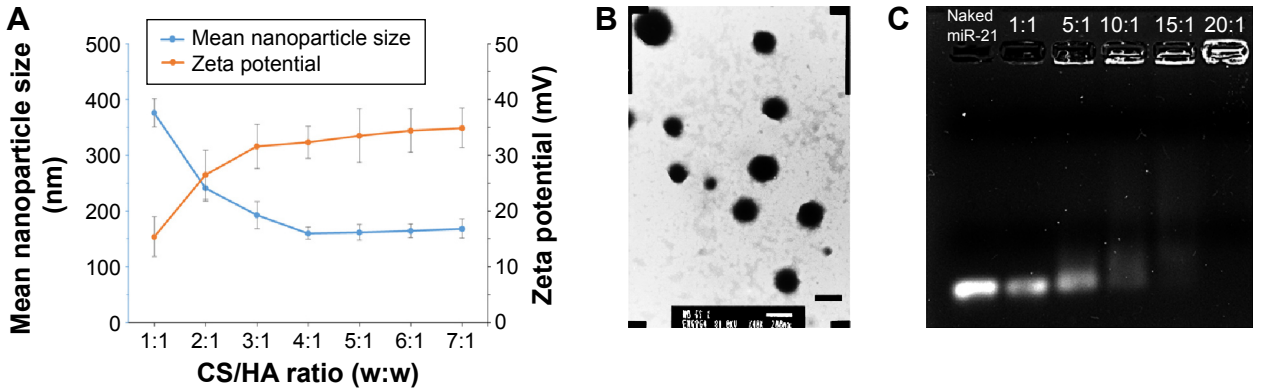

Figure 1 The characterizations of nanoparticles.
Notes: (**A**) Effect of the weight ratio of CS to HA on the particle size and zeta potential of HA/CS nanoparticles (n=3). (**B**) TEM images of HA/CS nanoparticles, bar =200 nm. (**C**) Gel retardation analysis of HA/CS/miR-21 nanoparticles; lane 1, naked miR-21; lanes 2–6, HA/CS/miR-21 nanoparticles prepared at N/P ratios of 1:1, 5:1, 10:1, 15:1, and 20:1.
Abbreviations: CS, chitosan; HA, hyaluronic acid; TEM, transmission electron microscopy; miR-21, microRNA-21.

The binding capacity of the CS/HA nanoparticles containing miRNA prepared at various N/P ratios was evaluated through a gel retardation assay. As shown in Figure 1C, the migrations of miR-21 in an agarose gel were completely retarded at an N/P ratio of 20:1, illustrating the complete combination of miR-21 with the CS/HA nanoparticles. For the subsequent study, we used CS/HA/miR-21 nanoparticles with a CS/HA ratio of 4:1 and an N/P ratio of 20:1.

Fabrication and surface morphology of miR-21-functionalized MAO Ti

Figure 2A and B show scanning electron microscopy (SEM) images of the MAO Ti surface morphology acquired through a pulsed direct-current power supply. After MAO, a porous morphology with evenly distributed 1–5 μm-diameter pores was obviously observed. This condition indicated that the pores formed by oxygen bubbles could provide an enlarged space for the attachment and loading of nanoparticles. Figure 2C–F show that the miR-21-loaded CS/HA nanoparticles were uniform and sleek, with diameters ranging from 50 to 200 nm, and formed a monolayer on the surfaces and micropores of the MAO Ti specimens. The images showed that a greater number of nanoparticles adherent to the pores compared with that found in the flat areas between the pores.

Fluorescence microscopy was used to evaluate the distributions of Cy3-labeled miR-21 and FITC-labeled CS, and the images demonstrated that both FITC-labeled CS (Figure 3A) and Cy3-labeled miR-21 (Figure 3B) were attached to the MAO Ti surface. The merged image (Figure 3C) presents a high degree of overlap, indicating that miR-21 was stably retained within the CS/HA nanoparticles after these were coated onto MAO Ti specimens.

Isolation and identification of hBMMSCs

Primary hBMMSCs were successfully obtained from a 22-year-old female volunteer, specifically from the drilled holes used for implant placement. The putative stem cells were characterized by their osteogenic/adipogenic differentiation potential and cell surface markers. The primary cells displayed a spindle-shaped morphology (Figure 4A). One of the key properties of any MSC line is a capacity for multiple-directional differentiation. Alizarin red S staining (Figure 4B) revealed alizarin red-positive mineralized nodules after 4 weeks of incubation, indicating the osteogenic potential of hBMMSCs. After 2 weeks of adipogenic induction, the cells were capable of forming microscopic oil red O-positive lipid droplets (Figure 4C), and the oil red O-positive cells provided strong evidence of their adipogenic differentiation. The immunophenotype of hBMMSCs was determined by flow cytometry (Figure 4D), and the results revealed that the cells were negative for hematopoietic markers, such as CD34 and CD45 and were positive for mesenchymal-associated markers, such as STRO-1 and CD146. In addition, STRO-1 was considered an early marker of MSCs. These results indicated that hBMMSCs were successfully obtained from the bone area used for implant placement.

Transfection efficiency of the miR-21-functionalized MAO Ti surface

To assess the ability of hBMMSCs to internalize the CS/HA/miR-21 nanoparticles, Cy3-labeled miRNAs and FITC-labeled CS were adopted to prepare CS/HA/miR-21 nanoparticles, which were applied in the coating process described in the "Materials and methods" section. Twenty-four hours after transfection, the internalized nanoparticles were located

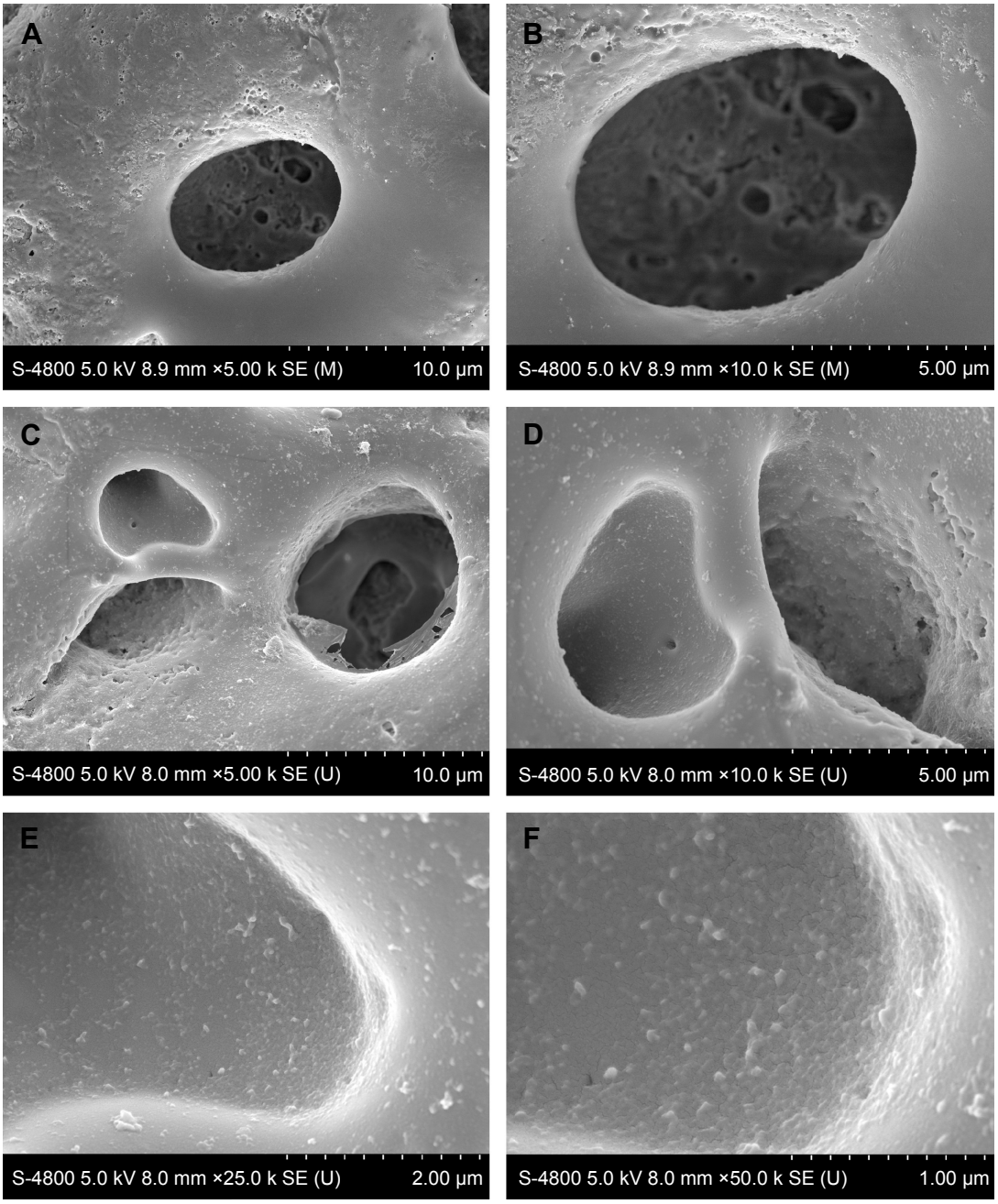

Figure 2 Morphology of the MAO Ti surfaces before and after HA/CS/miR-21 nanoparticle coating.
Notes: The morphology was assessed by SEM. (**A** and **B**) Different-magnification images of the naked MAO surface. (**C**–**F**) Images of the HA/CS/miR-21 nanoparticle-functionalized MAO surface at increasing magnification.
Abbreviations: CS, chitosan; HA, hyaluronic acid; SEM, scanning electron microscopy; MAO, microarc oxidation; miR-21, microRNA-21; Ti, titanium.

through fluorescent microscopy. The results clearly show that FITC-labeled CS (Figure 5B) and Cy3-labeled miR-21s (Figure 5C) were mainly located in the body of cells, with the nuclear regions (Figure 5A) exhibiting high levels of accumulation. The merged image (Figure 5D) shows a high degree of overlap between FITC-labeled CS and Cy3-labeled miR-21, indicating a stable settlement of miR-21 within the CS/HA nanoparticles. The merged image (Figure 5E) also shows a high degree of overlap between Cy3-labeled miR-21, FITC-labeled CS/HA nanoparticles, and a DAPI-labeled nucleus, indicating a high accumulation of nanoparticles in the nuclear regions.

Flow cytometry was employed to more accurately evaluate the transfection efficiency (Figure 5F). Different loading concentrations of miR-21 induced different transfection efficiencies. In total, the transfection efficiency increased in a dose-dependent

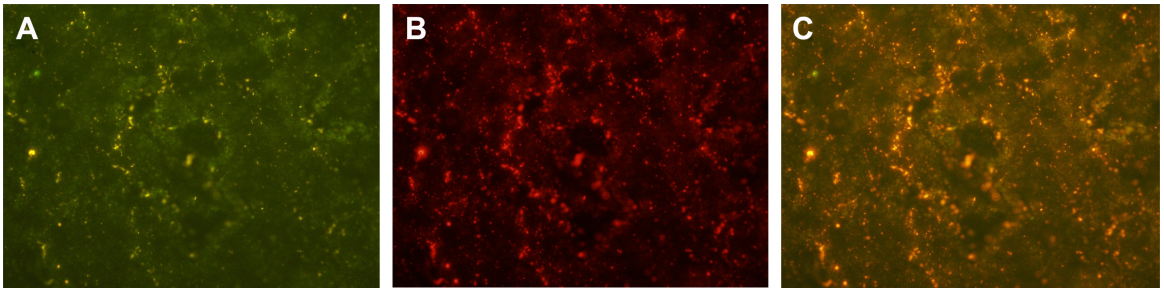

Figure 3 Fluorescence images of HA/CS/miR-21 nanoparticle-coated MAO surfaces.
Notes: (**A**) FITC-labeled chitosan (green), indicating the locations of CS/HA nanoparticles. (**B**) Cy3-labeled miR-21 (red). (**C**) Merged images.
Abbreviations: CS, chitosan; HA, hyaluronic acid; MAO, microarc oxidation; FITC, fluorescein isothiocyanate; miR-21, microRNA-21.

manner, and at a concentration of 450 pmol/specimen, the miR-21-functionalized MAO Ti surface achieved the highest transfection efficiency of more than 90%.

Cell viability and cytotoxicity

The effects of the different substrates on cell viability were measured using a CCK-8 kit. Comparable cell viability was observed (Figure 6A), and the results indicated that there were no statistically significant differences in the cell viability among the naked MAO surface, the vacant CS/HA nanoparticle-coated MAO surface, and the CS/HA/miR-21 nanoparticle-coated MAO surface ($P>0.05$).

The cytotoxicity of the different substrates was assessed by the LDH activity in the culture media 24 hours after transfection, and the results were compared in Figure 6B. Neither the substrates coated with vacant CS/HA nanoparticles nor the CS/HA/miR-21 nanoparticles exhibited any obvious cytotoxicity compared with the naked MAO surface ($P>0.05$).

Cell morphology

The photographs presented in Figure 7 show the morphologies of cells grown on different substrates, as determined by FE-SEM. In total, the cells grown on the miR-21-functionalized MAO Ti surface displayed a very similar cell morphology compared with those grown on the naked MAO surface. The cells spread well on both substrates, with abundant lamellipodia stretching out and covering the concave areas of the porous MAO Ti specimen, and also anchored themselves onto the surface through cell podia.

Expression of osteogenic genes

The expression levels of osteogenic genes, including *COLI*, *COLIII*, *RUNX2*, *OPN*, and *OCN*, were quantified by real-time

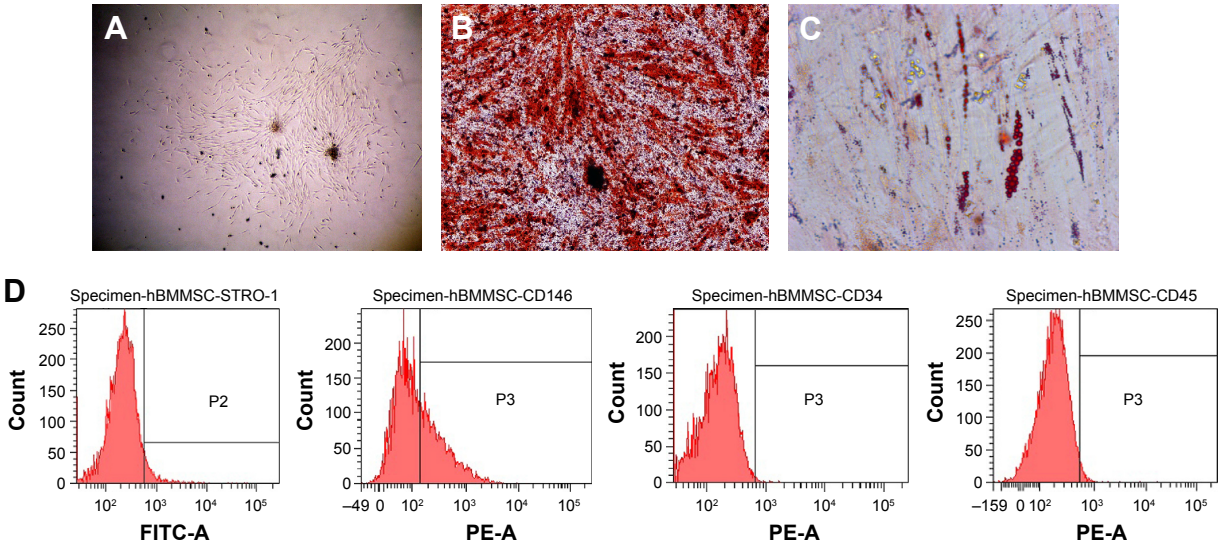

Figure 4 Isolation and characterization of hBMMSCs.
Notes: (**A**) The initial hBMMSCs were grown in six-well plates containing complete α-MEM. (**B**) Mineralized nodules were formed after 4 weeks of osteogenic induction (stained with alizarin red S, bar =100 μm). (**C**) Lipid vacuoles of different sizes and amounts were observed after 2 weeks of adipogenic induction (stained with oil red O, bar =200 μm). (**D**) Cytometric flow analysis indicated that the hBMMSCs expressed the positive mesenchymal-associated markers STRO-1 and CD146, but the cells were negative for the hematopoietic markers CD34 and CD45.
Abbreviations: hBMMSCs, human bone marrow mesenchymal stem cells; FITC, fluorescein isothiocyanate; α-MEM, Alpha Minimum Essential Medium; PE, phycoerythrin.

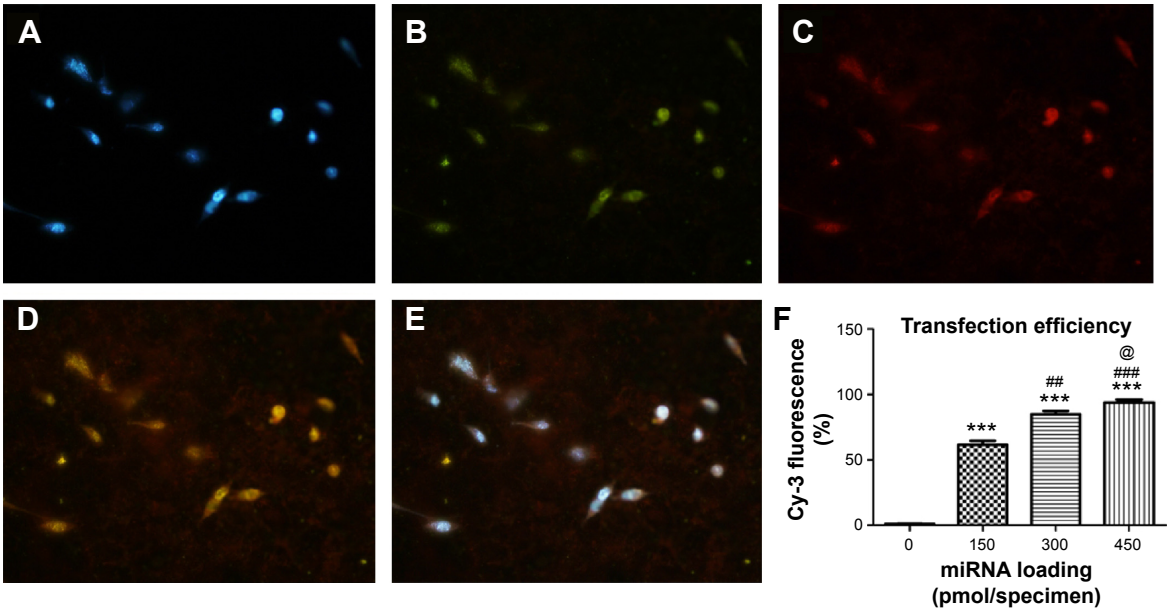

Figure 5 Uptake of HA/CS/miR-21 nanoparticles by cells.
Notes: Fluorescence images showing the cellular uptake of miR-21 after 24 hours of transfection in the reverse-transfection formulation of 450 pmol/specimen. (**A**) DAPI-labeled nuclei (blue). (**B**) FITC-labeled CS/HA nanoparticles. (**C**) Cy3-labeled miR-21 (red). (**D**) Merged images of (**B**) and (**C**). (**E**) Merged images of (**A**–**C**). (**F**) Comparison of the transfection efficiency among different specimens by flow cytometry. $^{***}P<0.001$ versus the naked MAO surface; $^{\#\#}P<0.01$ and $^{\#\#\#}P<0.001$ versus the 150 pmol miR-21 specimen group; $^{@}P<0.05$ versus the 300 pmol miR-21 specimen group.
Abbreviations: CS, chitosan; HA, hyaluronic acid; DAPI, 4′,6-diamidino-2-phenylindole; FITC, fluorescein isothiocyanate; miR-21, microRNA-21.

PCR (Figure 8). In general, different substrates induced different gene expression levels, which showed a time-dependent pattern and a dose-dependent effect. After 3 days of incubation, the 300 and 450 pmol groups showed higher expression levels of *OPN* and *OCN* than the other groups. At day 6, the highest gene expression levels of all five genes were found in the 450 pmol group, followed by the 300 and 150 pmol group. After culturing for 9 days, the 150, 300, and 450 pmol groups yielded higher expression levels of *RUNX2*, *OPN*, and *OCN* compared with that obtained in the naked MAO surface. These results reveal that the loading of miR-21 can effectively upregulate the expression of osteogenesis-related genes in vitro.

Discussion

The development of implants that induce robust osseointegration is a key clinical issue. Numerous studies have investigated the loading of therapeutic oligonucleotides (eg, DNA and siRNAs) onto biomaterials to promote this process at the genetic level,[33,34] whereas few such studies have investigated miRNAs, which have been proven to regulate the natural

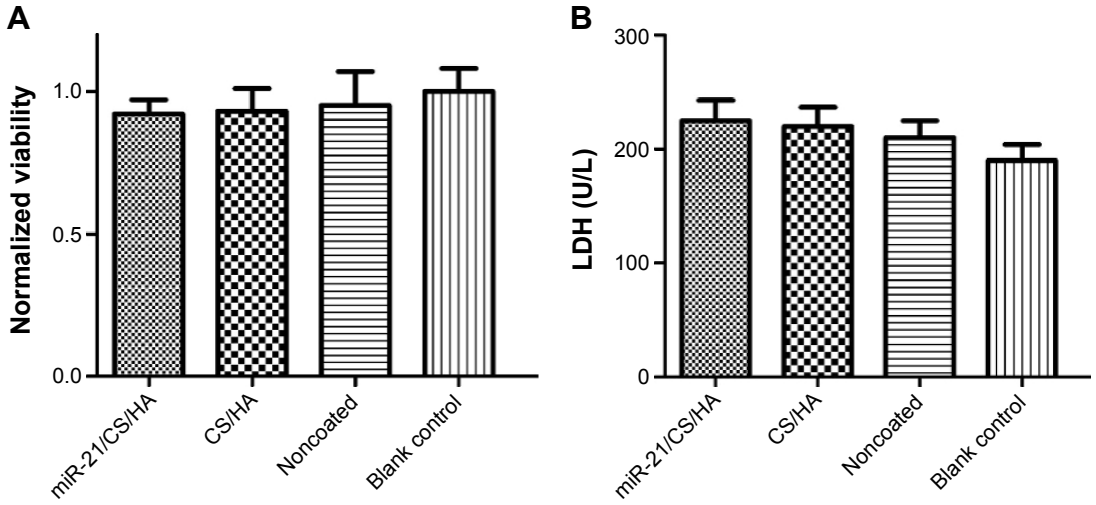

Figure 6 (**A**) Cell viability measured 24 hours after transfection by CCK-8. (**B**) LDH amount released by cells during the first 24 hours after transfection.
Abbreviations: CS, chitosan; HA, hyaluronic acid; miR-21, microRNA-21; LDH, lactate dehydrogenase.

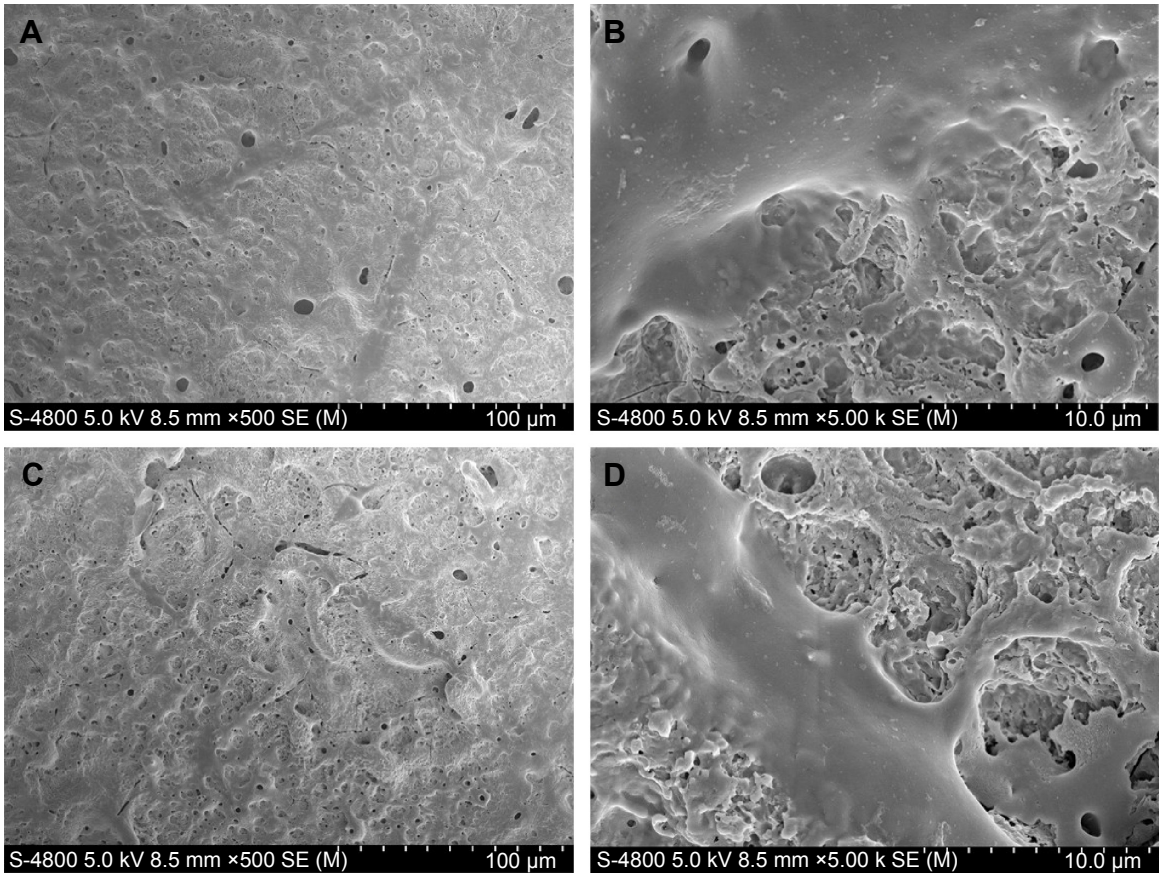

Figure 7 SEM images showing the cell morphology after 24 hours of incubation after transfection of different samples.
Notes: (**A** and **B**) Naked MAO surface. (**C** and **D**) HA/CS/miR-21 nanoparticle-functionalized MAO surface.
Abbreviations: CS, chitosan; HA, hyaluronic acid; MAO, microarc oxidation; miR-21, microRNA-21; SEM, scanning electron microscopy.

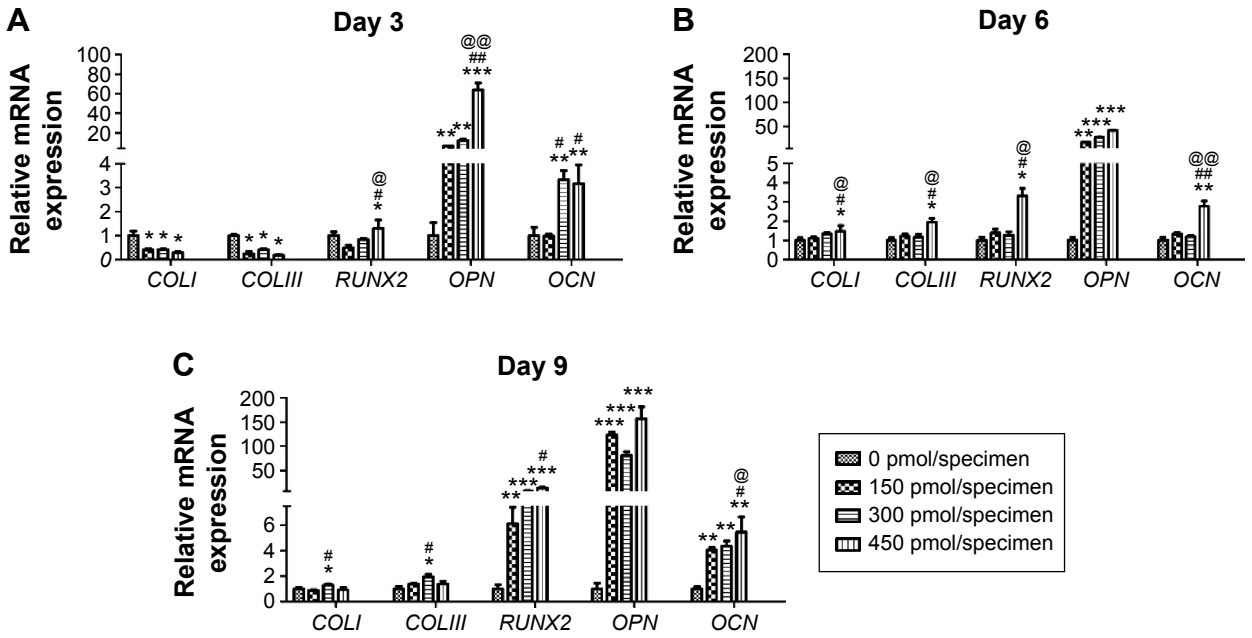

Figure 8 Relative expression levels of *COLI*, *COLIII*, *RUNX2*, *OPN*, and *OCN* by hBMMSCs cultured on different samples on days 3 (**A**), 6 (**B**), and 9 (**C**).
Notes: After transfection, the medium was changed to fresh medium, and the cells were cultured for another 24 hours. The medium was then changed to osteogenic medium, and the cells were cultured for 3, 6, and 9 days. All of the values were normalized to the GAPDH level. $^{*}P<0.05$, $^{**}P<0.01$, and $^{***}P<0.001$, respectively, versus the naked MAO surface; $^{\#}P<0.05$ and $^{\#\#}P<0.01$, respectively, versus the 150 pmol miR-21 specimen group; $^{@}P<0.05$ and $^{@@}P<0.01$, respectively, versus the 300 pmol miR-21 specimen group.
Abbreviations: hBMMSCs, human bone marrow mesenchymal stem cells; *COLI*, collagen type Iα1; *COLIII*, collagen type IIIα1; *RUNX2*, runt-related transcription factor 2; miR-21, microRNA-21; *OPN*, osteopontin; *OCN*, osteocalcin; *MAO*, microarc oxidation.

differentiation pathways of stem cells in vivo using a relatively less harmful strategy.[35] miR-21 has been widely studied and may induce the upregulation of the expression of osteogenesis-related genes.[16] In this work, we used CS/HA nanoparticles to stabilize, store, and deliver miR-21 in a controlled manner and explored appropriate CS/HA/miR-21 nanoparticles with a CS/HA ratio of 4:1 and N/P ratio of 20:1 for better transfection. We then fabricated CS/HA/miR-21 nanoparticle-coated MAO Ti surfaces through cross-linking using a 0.2% gel solution as a type of reverse transfection.[11,36] The miR-21-functionalized MAO Ti surfaces demonstrated comparable cell viability, cytotoxicity, and cell spreading to that exhibited by naked MAO Ti surfaces and induced a significantly higher expression of osteogenesis-related genes in hBMMSCs.

To identify a safe and efficient vector for gene delivery, we presented the development of a CS/HA nanocarrier system as a nonviral vector for transfection.[23,29] CS demonstrates many attractive advantages, including good biocompatibility, biodegradability, easy formulation into nanoparticles, and reasonable cost. However, the single application of CS has been shown to lack stability due to its low water solubility at physiological pH, which likely cannot efficiently protect miRNA, leading to the release of a large amount of miRNAs prior to endocytosis by the cells.[23] In this study, the inclusion of an anionic polymer (HA) increased the stability of the particles in plasma and increased the biocompatibility and gene transfection efficiency obtained in previous studies.[22,37] In addition, HA has the ability to bind to various cellular receptors, such as CD44, which is positively expressed in normal mammalian cells, including hBMMSCs.[22,38] This capability would induce the process and reduce side effects in a targeted manner. Liu et al[29] found that low-molecular-weight HA can improve cellular uptake through an interaction with the CD44 receptor[29] and lead to an easy release of the loaded transfection agents after cellular uptake.[28] In this study, HA was associated with CS through polyelectrolyte complexation and formed CS/HA nanoparticles with a CS/HA ratio of 4:1 and N/P ratio of 20:1. A significant decrease in nanoparticle size was found with increasing amounts of CS, and the smallest particle size (160.4±10.75 nm) was obtained at a CS:HA ratio of 4:1. The results were consistent with those obtained in previous studies,[23,28,29] which also found that nanoparticles with a relatively small particle size could be more easily internalized by cells. In addition, the nanoparticles with a CS:HA ratio of 4:1 presented a relatively high average zeta potential in our study, and this higher zeta potential also contributed to close contacts with the anionic membranes of cells.[28] In the gel retardation assay, the migration of miR-21 in an agarose gel was completely retarded at an N/P ratio of 20, illustrating the complete combination of miR-21 with the CS/HA nanoparticles. Therefore, we selected CS/HA/miR-21 nanoparticles with a CS/HA ratio of 4:1 and an N/P ratio of 20:1 for the subsequent study. In total, the results indicate that the nanoparticles are incorporated into the cells through the following mechanism: first, the relatively high zeta potential of the nanoparticles due to the presence of CS facilitates close contacts with the anionic membranes of cells; second, the HA components of the nanoparticles can bind specifically to the CD44 receptors of hBMMSCs; and third, the relatively smaller size of the nanoparticles also contribute to their internalization into cells. A previous study has demonstrated that HA is included in nonlysosomal vesicular compartments after cellular internalization and rapidly accumulates in the perinuclear region and cell nuclei.[39] In addition, HA is believed to act as a transcriptional activator likely by loosening the tight binding between miR-21 and the CS carrier, resulting in faster nucleic acid disassembly, thus favoring the upregulation of gene expression.[22]

As elaborated in the results, we successfully produced CS/HA/miR-21 nanoparticles and then used a 0.2% gel solution to cross-link the CS/HA/miR-21 nanoparticles onto the MAO Ti surface to produce a miR-21-functionalized MAO Ti surface. The SEM images showed that a greater number of nanoparticles retained in the pores than the surfaces due to the oscillating procedure used during fabrication; this design can thus effectively prevent the nanoparticles from falling off during plasmid insertion.[11] In addition, these micropores may provide a pool for the long-term transfection of CS/HA/miR-21 nanoparticles and reduce cytotoxicity.[11,40] This coating approach is simple and may be easily followed, showing its potential for clinical use. This study also demonstrated a relatively high level of transfection efficiency of more than 90%, which fulfills the criteria for gene transfection. This efficiency could be attributed to reverse transfection,[36,40] also known as substrate-mediated transfection. As designed in our study, CS/HA/miR-21 nanoparticles were immobilized onto a MAO Ti surface through cross-linking with a gel solution; therefore, the attached cells could directly contact the CS/HA/miR-21 nanoparticles. Compared with conventional transfection, reverse transfection delivers transfection agents locally, which facilitates their internalization and endocytosis by cells and reduces the amount of floating transfection agents in the culture medium.[34,36] The miR-21-functionalized MAO Ti surfaces displayed a high transfection effect, which was in line with previous reports of reverse transfection with siRNA.[41]

Excellent cytocompatibility is an elementary requirement of implants for clinical use, and our data demonstrate that the miR-21-functionalized MAO Ti surface fulfill this

requirement. In this study, both the naked and the miR-21-functionalized MAO Ti surfaces displayed similar cell viability and LDH secretion. This result may be ascribed to the CS/HA nanoparticles being safe and biocompatible vectors for clinical use, and the delayed release system also enabled a slow delivery of miRNA from the nanoparticles. The hBMMSCs used in this study are a type of anchorage-dependent cell, and good attachment plays an important role in regulating cell adhesion and the ensuing normal functions.[42] In this study, the cells displayed very similar cell spreading compared with cells grown on the naked MAO surface, as determined by SEM observations, and presented abundant cell lamellipodia stretching out on the Ti surface. The sufficient degree of cell spreading again indicates that the functionalized MAO Ti surface with CS/HA/miR-21 nanoparticles possess good cytocompatibility.

We used hBMMSCs to investigate the osteogenic ability of the miR-21-functionalized MAO Ti surface because these mimic the cells surrounding the bone implant biointerface obtained in vivo with the use of the miR-21-functionalized MAO Ti implants.[38] As expected, this new coating approach contributes to the differentiation process of hBMMSCs into osteoblasts. In this study, we found that the early markers of osteogenesis-related genes, including *COLI*, *COLIII*, *RUNX2*, *OPN*, and *OCN*, were upregulated compared with the levels obtained with the naked MAO Ti surface on days 3, 6, and 9, and this upregulation profile presented a time-dependent pattern and a dose-dependent effect. Our results indicated that the coating of CS/HA/miR-21 nanoparticles on the MAO Ti surface via reverse transfection promotes osteogenic differentiation at the mRNA level, which is in accordance with previous studies[16,17] that found that the overexpression of miR-21 can facilitate osteogenesis and accelerate bone fracture healing; furthermore, its target PI3K-AKT-GSK3β pathway may play an important role in the osteogenic differentiation of cells by stabilizing β-catenin according to previous reports.[17] This study confirmed the feasibility of fabricating CS/HA/miR-21 nanoparticle-coated MAO Ti surfaces via reverse transfection and demonstrated their application for the transfection of miR-21 to adjust the fate of hBMMSCs in vitro. The focus of our next study will be to determine the in vivo effects of this miR-21 coating method, including the induction of osseointegration between an implant and the surrounding bone.

Conclusion

In this work, we fabricated safe and biocompatible CS/HA nanoparticles as vectors for the delivery of miR-21 and successfully constructed CS/HA/miR-21 nanoparticles with a CS/HA ratio of 4:1 and N/P ratio of 20:1. The nanoparticles were then cross-linked with a 0.2% gel solution onto MAO-treated Ti surfaces to fabricate a CS/HA/miR-21 nanoparticle-coated MAO Ti surface. As a result, a novel coating for reverse transfection was developed. We successfully isolated and characterized hBMMSCs, and their biological effects, such as their effects on cell viability, cytotoxicity, and osteogenic gene expression of cells on the miR-21-functionalized MAO Ti surfaces, were evaluated. The results showed that cells on the miR-21-functionalized MAO Ti surfaces demonstrated cell viability, cytotoxicity, and cell spreading comparable to those exhibited by cells on the naked MAO Ti surfaces and presented a significantly higher expression of osteogenic genes. Therefore, these novel miR-21-functionalized MAO Ti implants may represent a potential design that could be used in the clinic to achieve more effective osseointegration.

Acknowledgments

This study was financially supported by the National Natural Science Foundation of China (grant number 81200823) and the Shaanxi Province Science and Technology Research and Development Project (2014K11-01-02-13). The authors appreciate the Department of Toxicology, the faculty of Preventive Medicine, the Fourth Military Medical University.

Author contributions

ZW and GW performed the experiments and wrote the main text of the manuscript. YZ, ZF, and ZW designed the experiments. YZ and ZF interpreted the results and revised the paper. All authors contributed toward data analysis, drafting and revising the paper and agree to be accountable for all aspects of the work.

Disclosure

The authors report no conflicts of interest in this work.

References

1. Ekelund JA, Lindquist LW, Carlsson GE, Jemt T. Implant treatment in the edentulous mandible: a prospective study on Brånemark system implants over more than 20 years. *Int J Prosthodont*. 2003;16(6):602–608.
2. Park J, Kim Y, Jang J, Kwon T, Bae Y, Suh J. Effects of phosphoric acid treatment of titanium surfaces on surface properties, osteoblast response and removal of torque forces. *Acta Biomater*. 2010;6(4):1661–1670.
3. Park J, Kim Y, Jang J, Song H. Osteoblast response to magnesium ion-incorporated nanoporous titanium oxide surfaces. *Clin Oral Implants Res*. 2010;21(11):1278–1287.
4. Li L, Kong Y, Kim H, et al. Improved biological performance of Ti implants due to surface modification by micro-arc oxidation. *Biomaterials*. 2004;25(14):2867–2875.
5. Wang YM, Jiang BL, Lei TQ, Guo LX. Microarc oxidation coatings formed on Ti6Al4V in Na2SiO3 system solution: microstructure, mechanical and tribological properties. *Surf Coat Tech*. 2006;201(1–2):82–89.

6. NIH Consensus Development Panel on Osteoporosis Prevention, Diagnosis, and therapy. Osteoporosis prevention, diagnosis, and therapy. *JAMA*. 2001;285(6):785–795.
7. Marco F, Milena F, Gianluca G, Vittoria O. Peri-implant osteogenesis in health and osteoporosis. *Micron*. 2005;36(7–8):630–644.
8. Wildemann B, Lübberstedt M, Haas NP, Raschke M, Schmidmaier G. IGF-I and TGF-beta 1 incorporated in a poly(d, l-lactide) implant coating maintain their activity over long-term storage – cell culture studies on primary human osteoblast-like cells. *Biomaterials*. 2004;25(17):3639–3644.
9. Wikesjö UME, Qahash M, Polimeni G, et al. Alveolar ridge augmentation using implants coated with recombinant human bone morphogenetic protein-2: histologic observations. *J Clin Periodontol*. 2008; 35(11):1001–1010.
10. Polimeni G, Wikesjö UME, Susin C, et al. Alveolar ridge augmentation using implants coated with recombinant human growth/differentiation factor-5: histologic observations. *J Clin Periodontol*. 2010;37(8):759–768.
11. Cheng Y, Wu J, Gao B, et al. Fabrication and in vitro release behavior of a novel antibacterial coating containing halogenated furanone-loaded poly(L-lactic acid) nanoparticles on microarc-oxidized titanium. *Int J Nanomed*. 2012;7(6):5641–5651.
12. Lund E, Güttinger S, Calado A, Dahlberg JE, Kutay U. Nuclear export of microRNA precursors. *Science*. 2004;303(5654):95–98.
13. Carthew RW, Sontheimer EJ. Origins and mechanisms of miRNAs and siRNAs. *Cell*. 2009;136(4):642–655.
14. Bushati N, Cohen SM. MicroRNA functions. *Annu Rev Cell Dev Biol*. 2007;23(1):175–205.
15. Papaioannou G, Lisse T, Kobayashi T. miRNAs in bone formation and homeostasis – microRNA in regenerative medicine. In: *MicroRNA in Regenerative Medicine*. Sen CK, editor. Waltham, MA: Academic Press; 2015:349–380.
16. Mei Y, Bian C, Li J, et al. miR-21 modulates the ERK-MAPK signaling pathway by regulating SPRY2 expression during human mesenchymal stem cell differentiation. *J Cell Biochem*. 2013;114(6):1374–1384.
17. Meng YB, Li X, Li ZY, et al. microRNA-21 promotes osteogenic differentiation of mesenchymal stem cells by the PI3K/β-catenin pathway. *J Orthop*. 2015;33(7):957–964.
18. Ourania T, Dimitra Z, Vasiliki B, et al. Sox2 suppression by miR-21 governs human mesenchymal stem cell properties. Stem cells. *Transl Med*. 2014;3(1):54–68.
19. El-Aneed A. An overview of current delivery systems in cancer gene therapy. *J Control Release*. 2004;94(1):1–14.
20. Gwak S, Jung JK, An SS, et al. Chitosan/TPP-hyaluronic acid nanoparticles: a new vehicle for gene delivery to the spinal cord. *J Biomater Sci Polymer Ed*. 2012;23(11):1437–1450.
21. Ragelle H, Riva R, Vandermeulen G, et al. Chitosan nanoparticles for siRNA delivery: optimizing formulation to increase stability and efficiency. *J Control Release*. 2014;176(3):54–63.
22. Ito T, Iida-Tanaka N, Niidome T, et al. Hyaluronic acid and its derivative as a multi-functional gene expression enhancer: protection from non-specific interactions, adhesion to targeted cells, and transcriptional activation. *J Control Release*. 2006;112(3):382–388.
23. Lu H, Zhao H, Wang K, Lv L. Novel hyaluronic acid-chitosan nanoparticles as non-viral gene delivery vectors targeting osteoarthritis. *Int J Pharm.* 2011;420(2):358–365.
24. Zheng F, Shi X, Yang G, et al. Chitosan nanoparticle as gene therapy vector via gastrointestinal mucosa administration: results of an in vitro and in vivo study. *Life Sci*. 2007;80(4):388–396.
25. Xin J, Chen T, Lin Z, Dong P, Tan H, Li J. Phosphorylated dendronized poly(amido amine)s as protein analogues for directing hydroxylapatite biomineralization. *Chem Commun*. 2014;50(49):6491–6493.
26. Wu D, Yang J, Li J, et al. Hydroxyapatite-anchored dendrimer for in situ remineralization of human tooth enamel. *Biomaterials*. 2013;34(21): 5036–5047.
27. Miyake K, Underhill CB, Lesley J, Kincade PW. Hyaluronate can function as a cell adhesion molecule and CD44 participates in hyaluronate recognition. *J Exp Med*. 1990;172(1):69–75.
28. Duceppe N, Tabrizian M. Factors influencing the transfection efficiency of ultra low molecular weight chitosan/hyaluronic acid nanoparticles. *Biomaterials*. 2009;30(13):2625–2631.
29. Liu Y, Kong M, Cheng XJ, Wang QQ, Jiang LM, Chen XG. Self-assembled nanoparticles based on amphiphilic chitosan derivative and hyaluronic acid for gene delivery. *Carbohydr Polym*. 2013;94(1): 309–316.
30. Knudson CB, Knudson W. Hyaluronan-binding proteins in development, tissue homeostasis, and disease. *FASEB J*. 1993;7(13):1233–1241.
31. Barlow S, Brooke G, Chatterjee K, et al. Comparison of human placenta- and bone marrow-derived multipotent mesenchymal stem cells. *Stem Cells Dev*. 2008;17(6):1095–1107.
32. Dominici M, Le Blanc K, Mueller I, et al. Minimal criteria for defining multipotent mesenchymal stromal cells. The International Society for Cellular Therapy position statement. *Cytotherapy*. 2006; 8(4):315–317.
33. Monaghan M, Pandit A. RNA interference therapy via functionalized scaffolds. *Adv Drug Deliver Rev*. 2011;63(4–5):197–208.
34. Jewell CM, Lynn DM. Surface-mediated delivery of DNA: cationic polymers take charge. *Curr Opin Colloid Interface Sci*. 2008; 13(6):395–402.
35. Eskildsen T, Taipaleenmaki H, Stenvang J, et al. MicroRNA-138 regulates osteogenic differentiation of human stromal (mesenchymal) stem cells in vivo. *Proc Natl Acad Sci U S A*. 2011;108(15):6139–6144.
36. Ziauddin J, Sabatini DM. Microarrays of cells expressing defined cDNAs. *Nature*. 2001;411(6833):107–110.
37. Mansouri S, Cuie Y, Winnik F, et al. Characterization of folate-chitosan-DNA nanoparticles for gene therapy. *Biomaterials*. 2006;27(9): 2060–2065.
38. Wagner W, Wein F, Seckinger A, et al. Comparative characteristics of mesenchymal stem cells from human bone marrow, adipose tissue, and umbilical cord blood. *Exp Hematol*. 2005;33(11):1402–1416.
39. Al-Qadi S, Alatorre-Meda M, Zaghloul EM, Taboada P, Remuñán-López C. Chitosan-hyaluronic acid nanoparticles for gene silencing: the role of hyaluronic acid on the nanoparticles' formation and activity. *Colloids Surf B Biointerfaces*. 2013;103:615–623.
40. Wu K, Song W, Zhao L, et al. MicroRNA functionalized microporous titanium oxide surface by lyophilization with enhanced osteogenic activity. *ACS Appl Mater Interfaces*. 2013;5(7):2733–2744.
41. Patil ML, Zhang M, Betigeri S, Taratula O, He H, Minko T. Surface-modified and internally cationic polyamidoamine dendrimers for efficient siRNA delivery. *Bioconjug Chem*. 2008;19(7):1396–1403.
42. Re F, Zanetti A, Sironi M. Inhibition of anchorage-dependent cell spreading triggers apoptosis in cultured human endothelial cells. *J Cell Biol*. 1994;127(2):537–546.